Bull. Chem. Soc. Jpn., 71, 355—362 (1998)

Rotational Predissociation Dynamics of H_2O ($\tilde{C}^1B_1$) by VUV Laser-Induced Photofragment Fluorescence Spectroscopy

Shilin Liu, Akiyoshi Hishikawa, and Kaoru Yamanouchi*

Department of Chemistry, School of Science, The University of Tokyo, 7-3-1 Hongo, Bunkyo-ku, Tokyo 113-0033

(Received September 19, 1997)

The rotational predissociation of water molecules in the vibrationless level of the $\tilde{C}^1B_1$ state was investigated under jet-cooled conditions (27—154 K) by exciting them with a tunable VUV laser in the wavelength range of 124.3—123.7 nm and by detecting the total fluorescence from electronically excited photofragments OH($A^2\Sigma^+$). Due to the simple one-photon selection rule and the efficient rotational cooling, individual low-J rotational transitions of the $\tilde{C}^1B_1$–$\tilde{X}^1A_1$ origin band were observed with almost no overlap in the laser-induced photofragment fluorescence (LIPF) spectrum. The widths and intensities of these rotational transitions exhibited pronounced dependence on the parent rotational levels in the $\tilde{C}^1B_1$ state. The least-squares analysis of the observed line-widths (FWHM) of the resolved rotational transitions, Γ's, showed that they are well described by the formula, $\Gamma = \Gamma_0 + \alpha_a\langle J_a'^2\rangle$, with optimized parameters $\Gamma_0 = 2.5(1)$ cm^{-1} and $\alpha_a = 0.63(1)$ cm^{-1}, indicating that (i) the homogeneous interaction couples the $\tilde{C}^1B_1$ state with the $\tilde{A}^1B_1$ state to form OH fragments in the electronically ground $^2\Pi_i$ state and (ii) the heterogeneous (a-axis orbital-rotation) interaction couples the $\tilde{C}^1B_1$ state with the $\tilde{B}^1A_1$ state to form OH fragments in the electronically excited $A^2\Sigma^+$ state. By taking account of the rotational line-broadening effect, the least-squares analysis was also performed to fit the observed spectral intensities to derive the branching ratio of the OH($A^2\Sigma^+$) formation via the $\tilde{B}^1A_1$ state of H_2O. It was found that the OH($A^2\Sigma^+$) formation branching ratio can be expressed by an exponential form, $\exp(-\gamma\langle J_a'^2\rangle)$, which was proposed first by Hodgson et al. [*Mol. Phys.*, **54**, 351 (1985)], and reproduces well the observed rotational intensity pattern when $\gamma = 0.097(7)$. By using this branching ratio and the previous data for the absorption oscillator strength, the absolute cross section to yield OH($A^2\Sigma^+$) photofragments was obtained as a function of the excitation energy.

The predissociation of water molecules with excitation energies below 10 eV has been studied intensively over the last few decades both experimentally[1—16] and theoretically.[17—24] In the long wavelength end of the vacuum ultraviolet (VUV) absorption spectrum, there are two broad and structureless absorption bands centered at 150 and 130 nm, which were assigned as the promotions: $3sa_1 \leftarrow 1b_1$ ($\tilde{A}^1B_1 \leftarrow \tilde{X}^1A_1$) and $3sa_1 \leftarrow 1a_1$ ($\tilde{B}^1A_1 \leftarrow \tilde{X}^1A_1$), from the ground electronic configuration.[3,4] In the shorter wavelength region of the absorption spectrum (124—119 nm), a diffuse absorption band exhibiting a distinct vibrational structure with a spacing around 1400 cm^{-1} was identified.[2] This structured absorption band was attributed to the bending progression of the $\tilde{C}^1B_1$–$\tilde{X}^1A_1$ transitions corresponding to the $3pa_1 \leftarrow 1b_1$ promotion. The dissociation rate at the origin band of the $\tilde{C}^1B_1$–$\tilde{X}^1A_1$ transition at 124 nm is known to be so slow that even its rotational structure can be resolved. The high resolution absorption measurements of the $\tilde{C}$–$\tilde{X}$ origin band[1] revealed that all the rotational lines are broadened due to predissociation induced by a rotationally dependent coupling of the $\tilde{C}^1B_1$ state to a singlet dissociative electronic state with A_1 symmetry.

Due to a difficulty in obtaining VUV radiation in the short wavelength region with a narrow bandwidth, the rotational predissociation in the $\tilde{C}^1B_1$ state has been studied so far only by multi-photon excitation spectroscopy. By using a pulsed dye laser, Ashfold et al.[5] and Kuge et al.[14] measured a (3+1)-resonantly enhanced multiphoton ionization (REMPI) excitation spectrum. On the other hand, by using a tunable KrF excimer laser, (i) Meijer et al.[8] measured a (2+1) REMPI spectrum, (ii) Hodgson et al.[9] measured a two-photon laser-induced fluorescence (LIF) spectrum by detecting fluorescence emitted from electronically excited photofragments OH($A^2\Sigma^+$), and (iii) Docker et al.[10] and Meijer et al.[8] measured a two-photon LIF spectrum by detecting the $\tilde{C}^1B_1 \rightarrow \tilde{A}^1B_1$ fluorescence emission of parent H_2O molecules.

These multiphoton studies showed that water molecules in the $\tilde{C}^1B_1$ state predissociate through homogeneous and heterogeneous pathways, affecting the rotational-line broadening in different ways. It has been argued that the rotationally independent predissociation proceeds through the homogeneous interaction with the dark $\tilde{A}^1B_1$ state to produce the electronic ground OH($X^2\Pi_i$),[5,10,13] and the rotationally dependent predissociation is caused by the heterogeneous (orbital-rotation) interaction between the excited $\tilde{C}^1B_1$ state and the unbound $\tilde{B}^1A_1$ state. It has been known that a further branching occurs once the molecules are prepared in the $\tilde{B}^1A_1$ state. So far, three different fragmentation channels through the $\tilde{B}^1A_1$ state have been discussed. The first

one is an adiabatic pathway to produce electronically excited photofragments, $OH(A^2\Sigma^+)$.[3—18] The second and third pathways produce electronic ground photofragments, $OH(X^2\Pi_i)$ through non-adiabatic couplings at linear configurations, i.e. the Renner–Teller interaction with the $\tilde{A}^1B_1$ state and the coupling with the $\tilde{X}^1A_1$ state through the conical intersection.[20] In summary, the proposed complicated predissociation pathways of H_2O from the $\tilde{C}^1B_1$ state can be described as follows:

$$H_2O(\tilde{C}^1B_1) \xrightarrow{\text{rotation-independent}} H_2O(^1B_1 \text{ dark channel}) \longrightarrow OH(X^2\Pi_i) + H \quad (1a)$$

$$H_2O(\tilde{C}^1B_1) \xrightarrow{\text{orbital-rotation}} H_2O(\tilde{B}^1A_1) \xrightarrow{\text{adiabatic}} OH(A^2\Sigma^+) + H \quad (1b)$$

$$H_2O(\tilde{C}^1B_1) \xrightarrow{\text{Renner - Teller}} H_2O(\tilde{A}^1B_1) \longrightarrow OH(X^2\Pi_i) + H \quad (1c)$$

$$H_2O(\tilde{C}^1B_1) \xrightarrow{\text{conical}} H_2O(\tilde{X}^1A_1) \longrightarrow OH(X^2\Pi_i) + H \quad (1d)$$

If the rotational structure of the $\tilde{C}$–$\tilde{X}$ band is measured with sufficiently high resolution, the contribution from the rotationally dependent and rotationally independent predissociation pathways could be clarified through the widths and intensities of the individual rotational transitions. In the previous studies, the rotational structure of the $\tilde{C}$–$\tilde{X}$ origin band was measured under bulb conditions at room temperature, and therefore, the rotational transitions overlap with each other to form an only partially resolved rotational structure. Furthermore, in the case of multiphoton laser spectroscopy, relative intensities of spectral peaks are affected sensitively by the fluctuation of the laser intensity. In the present study, in order to clarify the complex dissociation mechanism in the $\tilde{C}^1B_1$ state of H_2O, we measured for the first time one-photon excitation spectra of the $\tilde{C}^1B_1 \leftarrow \tilde{X}^1A_1$ origin band under jet-cooled conditions using a tunable vacuum ultraviolet (VUV) laser with a narrow bandwidth (ca. 0.4 cm^{-1}). In the measurements of the excitation spectra, the fluorescence emitted from the $OH(A^2\Sigma^+)$ photofragments was monitored. We hereafter call this type of an excitation spectrum, in which fluorescence is emitted from electronically excited photofragments produced after photodissociation, a laser-induced photofragment fluorescence (LIPF) spectrum.

Experimental

The tunable VUV laser light was generated by two-photon resonant four-wave difference frequency mixing in Kr by the scheme denoted as $\omega_{VUV}=2\omega_{UV}-\omega_{IR}$,[26] where ω_{VUV}, ω_{UV}, and ω_{IR} represent wavenumbers of the laser output in the VUV, UV, and near-IR regions, respectively. The UV output, tuned to the two-photon resonant transition to Kr 5p[5/2,2] at 92308.2 cm^{-1}, was generated by the BBO doubling of the output of a pulse-dye laser (Lambda Physik Scanmate 2EY) pumped by the THG (354.7 nm) output of a Nd : YAG laser (Coherent Infinity 40-100). An idler output, ω_{IR}, with a bandwidth of 0.2 cm^{-1} of an optical parametric oscillator (OPO) laser (Lambda Physik OPPOE) pumped by the same THG output of the Nd : YAG laser was tuned in the range of 848—868 nm.

Both of the laser beams for ω_{UV} and ω_{IR} were merged co-axially by a dichroic mirror, and were focused by an achromatic lens with $f=300$ mm into a frequency conversion cell containing Kr gas (1—2 Torr, 1 Torr=133.322 Pa), with an appropriate amount of Ar added as a positively dispersive buffer gas. The generated VUV light in the 124.3—123.7 nm range, which covers the origin band of the $\tilde{C}^1B_1 \leftarrow \tilde{X}^1A_1$ transition of H_2O, was separated from the incident ω_{UV} and ω_{IR} laser beams by an LiF prism. The VUV light beam crossed perpendicularly with the supersonic jet of the sample gas (H_2O, 1.5% in He) expanded from a pulsed nozzle (General Valve 9-279-900). The total fluorescence emitted from the excited photofragments $OH(A^2\Sigma^+)$ was detected by a photomultiplier (Hamamatsu R928) placed in the direction perpendicular to both the jet axis and the VUV light beam. The signal from the photomultiplier was amplified by a preamplifier (NF BX-31) and averaged by a boxcar integrator (Stanford SR250). Commercial deionized and distilled water (Bio Whittaker) was used without further purification. Different rotational temperatures (27—80 K) of H_2O were achieved by changing the stagnation pressure (250—900 Torr) and the laser-nozzle distance (X/D=4—12). Higher rotational temperatures above 100 K were achieved by interrupting the free jet expansion with a stainless steel mesh (#25) sheet placed at about 1 mm distance from the nozzle orifice. The VUV laser intensity was simultaneously monitored with a solar-blind photomultiplier (Hamamatsu R1259) by reflecting a part of the VUV laser with a quartz plate. The LIPF spectra were obtained by scanning the VUV-laser wavelength, and by normalizing the VUV intensity. The wavelength of the generated VUV light was calibrated by the laser-induced fluorescence (LIF) spectrum of the $A^1\Pi$–$X^1\Sigma^+$ (12, 0) transition of CO at 124.6 nm.[25] By the simulation of the rotational structure of the CO transition, the resolution of the VUV light was estimated to be 0.4 cm^{-1}. The experimental details for spectroscopic measurements using a tunable VUV laser light were also described in our recent papers.[26—28]

Results and Discussion

1. Rotational Effect in Line Broadening. The rotational structure of the VUV LIPF spectra of the $\tilde{C}$–$\tilde{X}$ origin band of H_2O exhibited a sensitive dependence on the expansion conditions, reflecting changes in the rotational temperatures. In Fig. 1, two typical free jet spectra with different expansion conditions are shown. The rotational temperatures for the lower and upper traces derived from the spectral simulation described below are 27 and 154 K, respectively. Previously, the high resolution absorption spectrum of the $\tilde{C}$–$\tilde{X}$ origin band of H_2O was measured by Johns[1] under bulb conditions at room temperature, and the rotational assignments were performed to determine the rotational constants of the vibrational ground level, i.e. $(v_1,v_2,v_3)=(0,0,0)$, of the $\tilde{C}^1B_1$ state, where v_1,v_2, and v_3 denote vibrational quantum numbers for the v_1 (symmetric stretch), v_2 (bend), and v_3 (anti-symmetric stretch) modes, respectively. By using the rotational constants reported by Johns, the assignments of the rotational transitions in the present LIPF spectra were performed straightforwardly, as shown in Fig. 1 in the form of $J'_{Ka'Kc'}-J''_{Ka''Kc''}$. The band origin was determined to be 80624.6(4) cm^{-1} from the spectral simulations as described below, with the wavelength of the excitation VUV light calibrated by the LIF spectrum of the A–X (12,0) band of CO. Due to the low rotational temperatures achieved under the jet-cooled conditions, the rotational transitions between the levels having low-rotational quantum numbers were clearly identified with almost no overlap with other high-J rotational

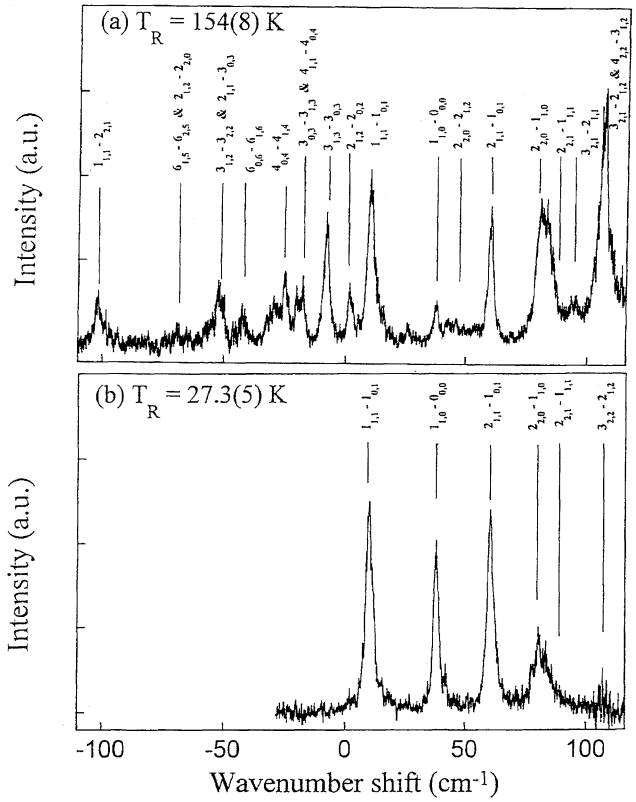

Fig. 1. Laser-induced photofragment fluorescence (LIPF) spectra of the origin band of the $\tilde{C}^1B_1$–$\tilde{X}^1A_1$ transition of H_2O at (a) 154 K and (b) 27 K. Rotational assignments are shown in the form of $J'_{Ka'Kc'} - J''_{Ka''Kc''}$. The wavenumber shift is measured from the band origin at 80624.6(4) cm^{-1}, which was derived from the least-squares fits to the five LIPF spectra (see Section 2).

transitions.

Since the previous three-photon and two-photon resonance excitation spectra were measured under bulb conditions at room temperature, many rotational transitions overlap with each other. Furthermore, the complex selection rules in the multi-photon process increase the number of rotational transitions. As a consequence, the excitation spectra exhibited only a partially resolved rotational structure. In contrast, the present LIPF spectra, in which the low-J transitions are observed with almost no overlap, afforded a valuable basis to investigate the J-dependent predissociation process through the widths and intensities of the individual rotational transition peaks.

It can be noticed in Fig. 1 that the widths of the rotational transitions vary sensitively depending on the rotational levels of the $\tilde{C}^1B_1$ state involved. The linewidths of isolated peaks which are formed by a single rotational transition were measured and are listed in Table 1. Since the rotationally independent and rotationally dependent dissociation pathways are expected to contribute to the observed transition line-broadening, the line-width Γ of the respective rotational transitions is expressed as:

$$\Gamma = \Gamma_0 + \Gamma_{rot}, \tag{2}$$

Table 1. Observed Linewidths for Isolated Rotational Transitions of the $\tilde{C}^1B_1$–$\tilde{X}^1A_1$ Origin Band of H_2O

Transition	Position	Width/cm^{-1}	
	cm^{-1}	Obsd	Calcd[a)]
$1_{1,0}$–$0_{0,0}$	80662.9	2.9(3)	3.13
$1_{1,1}$–$1_{0,1}$	80635.2	3.2(1)	3.13
$1_{1,1}$–$2_{2,1}$	80524.2	3.1(2)	3.13
$2_{1,1}$–$1_{0,1}$	80685.4	3.1(1)	3.13
$2_{1,2}$–$2_{0,2}$	80626.9	3.0(2)	3.13
$3_{1,3}$–$3_{0,3}$	80617.2	2.9(3)	3.14
$2_{2,0}$–$1_{1,0}$	80707.1	5.0(1)	4.97
$3_{2,1}$–$2_{1,1}$	80719.1	4.9(2)	4.86
$4_{0,4}$–$4_{1,4}$	80600.6	2.6(2)	2.82
$6_{0,6}$–$6_{1,6}$	80583.5	3.0(1)	3.24

a) Calculated by the formula $\Gamma = \Gamma_0 + \alpha_a \langle J'^2_a \rangle$ with the optimized parameters, Γ_0=2.5 cm^{-1} and α_a=0.63 cm^{-1}, obtained by the least-squares fit to the observed peak widths.

where Γ_0 and Γ_{rot} represent the line broadening caused by the rotationally independent and dependent dissociation pathways, respectively. The line broadening caused by the rotationally dependent process should be proportional to the sum of the square modulus of matrix elements of a rotationally dependent Hamiltonian, H_{rot}, between a certain rovibronic level $|\Psi_i(\tilde{C})\rangle$ in the $\tilde{C}^1B_1$ state and all possible rovibronic levels, $\{|\Psi_k(d)\rangle\}$, of a dissociative electronic state, i.e.,

$$\Gamma^i_{rot} \propto \sum_k |\langle \Psi_k(d)|H_{rot}|\Psi_i(\tilde{C})\rangle|^2. \tag{3}$$

When an orbital-rotation coupling is assumed as an origin of the rotationally dependent interaction, the Hamiltonian can be written using effective rotational constants, A, B, and C, as

$$H_{rot} = -2AL'_aJ'_a - 2BL'_bJ'_b - 2CL'_cJ'_c, \tag{4}$$

where projections of the electronic and total angular momenta in the $\tilde{C}^1B_1$ state onto an inertial q (q=a,b, or c) axis are denoted as L'_q and J'_q, respectively. Since J'_a, J'_b, and J'_c operate only on the rotational parts, $|\Phi_i(\tilde{C})\rangle$ and $|\Phi_k(d)\rangle$, of the total wavefunctions under the Born–Oppenheimer approximation, $|\Psi_i(\tilde{C})\rangle$ and $|\Psi_k(d)\rangle$, respectively, Γ^i_{rot} for the i-th rotational level in Eq. 3 is expressed as a linear combination of three terms representing orbital-rotational interaction, i.e.,

$$\Gamma^i_{rot,q} \propto \sum_k |\langle \Phi_k(d)|J'_q|\Phi_i(\tilde{C})\rangle|^2 = \langle \Phi_i(\tilde{C})|J'^2_q|\Phi_i(\tilde{C})\rangle \equiv \langle J'^2_q\rangle_i. \quad q = a,b,c \tag{5}$$

Finally, the linewidth of a given rotational level in the $\tilde{C}$ state is expressed as

$$\Gamma^i = \Gamma^i_0 + \sum_q \Gamma^i_{rot,q} = \Gamma^i_0 + \alpha_a\langle J'^2_a\rangle + \alpha_b\langle J'^2_b\rangle + \alpha_c\langle J'^2_c\rangle, \tag{6}$$

where α_a, α_b, and α_c are coefficients representing magnitudes of the orbital-rotation interactions around the a, b, and c-axis, respectively.

For an asymmetric top molecule like H_2O, K'_a and K'_c are not good quantum numbers, and the expectation values of $\langle J'^2_a\rangle$, $\langle J'^2_b\rangle$, and $\langle J'^2_c\rangle$ should be used to describe the rotational dependence of the line-width. The expectation values of $\langle J'^2_a\rangle$, $\langle J'^2_b\rangle$, and $\langle J'^2_c\rangle$ were evaluated using the rotational constants given by Johns.[1] In principle, the four parameters in Eq. 6 could be determined from the measurements of the line-widths of different rotational levels. However, as can be seen in Fig. 2, where the measured line-widths listed in Table 1 are plotted as a function of $\langle J'^2_a\rangle$ with bars representing the uncertainty, the line-width depends almost linearly on $\langle J'^2_a\rangle$. Therefore, by assuming that the contribution from the a-axis orbital-rotation interaction is dominant, a least-squares fit to the formula

$$\Gamma = \Gamma_0 + \alpha_a\langle J'^2_a\rangle, \tag{7}$$

was performed. From the least-squares fit, the optimized parameters, Γ_0=2.5(1) cm^{-1} and α_a=0.63(1) cm^{-1}, were obtained. The best-fit straight line drawn in Fig. 2 using these optimized parameters reproduces well the observed line widths with small residuals, as listed in Table 1, indicating that rotationally dependent line broadenings are caused mainly by the a-axis orbital-rotation interaction.

Since the a-axis rotation has b_1 symmetry in the C_{2v} point group to which H_2O molecules belong, the dissociative electronic state which the $\tilde{C}^1B_1$ state is coupled with by the a-axis orbital-rotation interaction should have A_1 symmetry ($b_1\times B_1=A_1$). The observed rotational dependence in the predissociative $\tilde{C}^1B_1$ state shows clearly that the excited photofragments OH($A^2\Sigma^+$) are generated via two sequential processes: (i) the $\tilde{C}^1B_1$ state couples with the dissociative $\tilde{B}^1A_1$ state through the a-axis orbital-rotation interaction, and (ii) the dissociation occurs on the potential energy surface (PES) of the $\tilde{B}^1A_1$ state to produce OH(A) fragments.

2. Branching Ratios of Dissociation Channels. From the relative intensities of the rotational transition peaks in the LIPF spectrum, information about the dissociation branching ratios can be derived. The branching ratio to produce OH(A) can be written as a product of the branching ratios for the two sequential processes, by assuming that there is no coherent interference between these channels. The branching ratio β_1 of the first process is expressed as the relative contribution of the rotationally dependent broadening to the total broadening, i.e.,

$$\beta_1 = \frac{\alpha_a\langle J'^2_a\rangle}{\Gamma_0 + \alpha_a\langle J'^2_a\rangle}. \tag{8}$$

Since the two parameters, Γ_0 and α_a, were determined in Section 1 for the $\tilde{C}$–$\tilde{X}$ origin band, the branching ratios, β_1s, for all the rotational levels in the $\tilde{C}^1B_1(0,0,0)$ vibrational ground level were evaluated using Eq. 8. If the subsequent dissociation to form OH(A) fragments is assumed to be a rotationally independent process, the LIPF spectra can be simulated by multiplying β_1s and the rotational transition intensities. However, the LIPF spectra simulated in this manner were found to give considerably larger spectral intensities for high-J transitions than in the observed LIPF spectra, indicating that the second process to produce OH(A) fragments is largely decelerated by the rotational excitation in the parent H_2O molecules. In order to account for the rotationally dependent deceleration process, the branching ratio β_2 for the second process having an exponential decay form,

$$\beta_2 = e^{-\gamma\langle J'^2_a\rangle}, \tag{9}$$

was introduced with a variable parameter γ. The exponential decay form was first introduced by Hodgson et al.[9] to describe the second branching ratio.

In the least-squares fit of the observed rotational intensity pattern of the LIPF spectra, a total of five parameters: γ, T_R (rotational temperature), ω_0 (rotational band origin wavenumber), Δ (baseline shift of the measured spectra), and C_0 (normalization factor) were adopted as independent parameters. The calculated rotational structure of the spectrum is described using these five parameters as,

$$I_{calcd}(\omega) = C_0\sum_i\left[I_i^0(\omega_i,T_R)\frac{\alpha_a\langle J'^2_a\rangle}{\Gamma_0+\alpha_a\langle J'^2_a\rangle}e^{-\gamma\langle J'^2_a\rangle}L(\omega,\omega_i-\omega_0)\right]+\Delta, \tag{10}$$

where $I_i^0(\omega_i,T_R)$ represents the relative intensity of the i-th rotational transition at transition wavenumber ω_i evaluated at a rotational temperature T_R using the rotational constants of the $\tilde{X}^1A_1$ (0,0,0)[29] and $\tilde{C}^1B_1$ (0,0,0)[1] levels with nuclear spin statistical weights (ee : eo : oo : oe=1 : 3 : 1 : 3). The Boltzmann distributions were assumed here for the rotational levels in the $\tilde{X}^1A_1(0,0,0)$ of the parent H_2O. The line profile $L(\omega,\omega_i)$ represents a normalized Lorentzian function,

$$L(\omega,\omega_i) = \frac{\Gamma/2\pi}{(\omega-\omega_i)^2+(\Gamma/2)^2}, \tag{11}$$

where $\Gamma=\Gamma_0+\alpha_a\langle J'^2_a\rangle$ denotes the rotational line-width evaluated using the two known parameters, Γ_0 and α_a.

The LIPF spectra were measured under five different expansion conditions, as shown in Fig. 3. It can be seen clearly

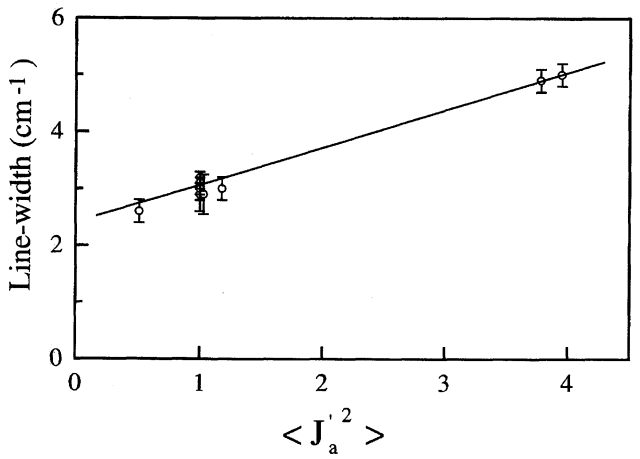

Fig. 2. The least-squares fit of the measured line-width Γ to the formula $\Gamma=\Gamma_0+\alpha_a\langle J'^2_a\rangle$. The two optimized parameters, Γ_0=2.5(1) cm^{-1} and α_a=0.63(1) cm^{-1}, were determined from the fit.

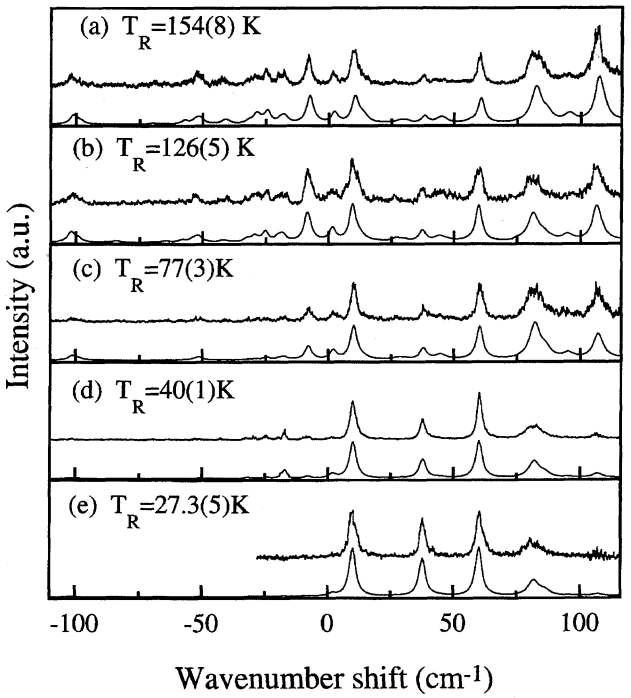

Fig. 3. Laser-induced photofragment fluorescence (LIPF) spectra of H_2O at different rotational temperatures, and their calculated best-fit spectra. These five spectra measured under different expansion conditions, (a)—(e), are presented by the increasing order of their rotational temperatures from the lower to the upper traces. The wavenumber shift is measured from the band origin at 80624.6(4) cm^{-1}.

that the intensity pattern of the LIPF spectra changes sensitively with temperature; i.e., at low temperatures, only a few isolated peaks are identified, while by increasing the temperature the number of transition peaks having detectable intensities increases significantly. The least-squares fits were performed to the 2000—5000 intensity data at equally spaced wavenumber positions in the five observed spectra. It was found that the five parameters were determined with only small uncertainties in all the five LIPF spectra. The optimized values of T_R, γ, and ω_0 determined for the respective five LIPF spectra (a)—(e) are listed in Table 2. As an average value of the five band origin data, the rotational band origin of the $\tilde{C}(0,0,0)$–$\tilde{X}(0,0,0)$ transition was determined to be 80624.6(4) cm^{-1}, which is consistent with that derived by Johns,[1] 80624.7(6) cm^{-1}, from a high-resolution absorption spectrum measured at room temperature. The best-fit spectra using the optimized parameters are also presented in Fig. 3 with the observed LIPF spectra. All the five figures (Fig. 3(a)—(e)) show both the relative intensities and the line-widths of the transition peaks in the best-fit spectra are in excellent agreement with the observed spectra, indicating that the assumed exponential form for the branching ratio β_2 to form excited $OH(A^2\Sigma^+)$ photofragments is appropriate. The determined γ values were plotted as a function of the rotational temperature T_R, as shown in Fig. 4, in which the horizontal and vertical bars represent the uncertainties of T_R and γ, respectively. As can been seen in Fig. 4, γ is almost independent of the rotational temperature T_R. The averaged value of γ was then determined to be γ=0.097(7).

Table 2. Optimized Parameters, T_R, γ, and ω_0, Obtained by the Least-Squares Fit to the Rotationally Resolved LIPF Spectra in Fig. 3

Spectra in Fig. 3	T_R (K)	γ	ω_0 (cm^{-1})
(a)	154(8)	0.09(3)	80624.5(7)
(b)	126(5)	0.10(2)	80624.1(7)
(c)	77(3)	0.09(2)	80624.9(5)
(d)	40(1)	0.10(3)	80624.8(7)
(e)	27.3(5)	0.11(3)	80624.7(7)
Average values		0.097(7)	80624.6(4)

Since we have determined both the first branching ratio β_1 to couple the $\tilde{C}^1B_1$ state with the $\tilde{B}^1A_1$ state and the second branching ratio β_2 to form OH(A) photofragments, the branching ratios for competing dissociation Channels (1a), (1b), and (1c)+(1d) mentioned in the introduction part can be expressed as:

$$\text{Channel (1a)} \qquad P_a = \frac{\Gamma_0}{\Gamma_0 + \alpha_a \langle J_a'^2 \rangle}, \tag{12}$$

$$\text{Channel (1b)} \qquad P_b = \frac{\alpha_a \langle J_a'^2 \rangle}{\Gamma_0 + \alpha_a \langle J_a'^2 \rangle} e^{-0.097 \langle J_a'^2 \rangle}, \tag{13}$$

$$\text{Channel (1c)+(1d)} \qquad P_{c,d} = \frac{\alpha_a \langle J_a'^2 \rangle}{\Gamma_0 + \alpha_a \langle J_a'^2 \rangle} (1 - e^{-0.097 \langle J_a'^2 \rangle}). \tag{14}$$

The branching ratios for these dissociation channels depend sensitively on the rotational quantum number as plotted in Fig. 5 as a function of $\langle J_a'^2 \rangle^{1/2}$. For rotational levels with low $\langle J_a'^2 \rangle^{1/2}$, the main contributions come from the rotationally independent dissociation [Channel (1a)] and the OH(A) generation [Channel (1b)] pathways. But for levels with high $\langle J_a'^2 \rangle^{1/2}$, contributions from Channels (1a) and (1b) decrease,

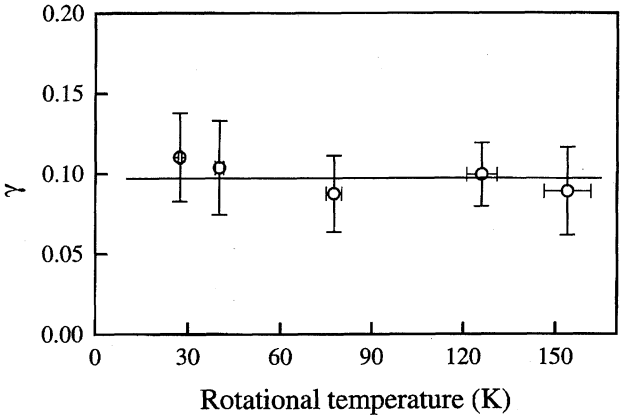

Fig. 4. The rotational temperature T_R and the γ parameter in the branching ratio form $\exp(-\gamma\langle J_a'^2 \rangle)$ determined from the least-squares fitting to the five observed spectra measured under the different expansion conditions. The horizontal and vertical bars represent the uncertainties for T_R and γ, respectively. The horizontal straight line represents an average value of γ=0.097(7) obtained as a simple average over the five different γ's.

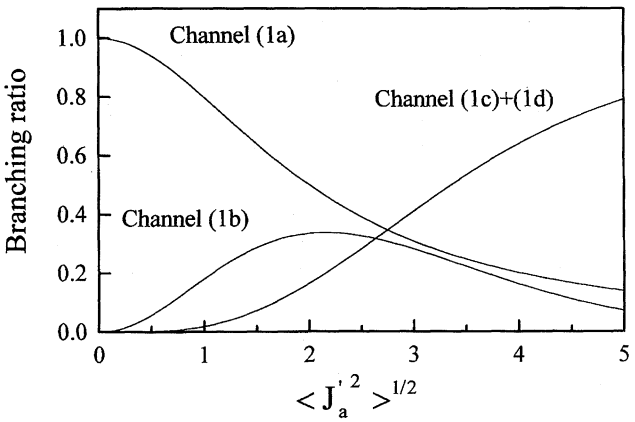

Fig. 5. The branching ratios for the dissociation channels (1a), (1b), and (1c)+(1d) as a function of $\langle J_a'^2\rangle^{1/2}$ obtained from Eqs. 12, 13, and 14.

and in turn, that from Channel (1c)+(1d) increases. Therefore, it can be said that the main dissociation pathways become different for different rotational temperatures. At very low T_R, (1a) and (1b) are the main dissociation channels, while at higher T_R, (1c)+(1d) becomes a main dissociation channel.

3. Comparison with Previous Studies. Previously, Γ_0 and C_a in the line-width expression, $\Gamma=\Gamma_0(1+C_a\langle J_a'^2\rangle)$[8,14] or $\Gamma=\Gamma_0(1+C_aK_a'^2)$,[5,14] were determined as listed in Table 3, where C_a were transformed into $\alpha_a=\Gamma_0C_a$ for the comparison with our results. As clearly shown in this table, the Γ_0 and α_a values obtained from the rotational contour analysis of the two-photon LIF spectrum (Ref. 8) are consistent with ours within their experimental uncertainties, though these parameters were obtained via a trial-and-error procedure. Considering the fact that their experiments were performed at room temperature, this agreement between our parameters and theirs indicates that the line-width formula of Eq. 7 with our parameters obtained from the low-K_a' transitions is also applicable to describe the line-widths of the high-K_a' rotational transitions.

In Ref. 5, the parameters were obtained from the trial-and-error rotational contour analysis of the (3+1)-REMPI excitation spectrum measured at room temperature, but the uncertainties associated with the estimated parameters were not reported. On the one hand, Γ_0 and α_a were determined in Ref. 14 from the observed rotational line-widths in the (3+1)-REMPI excitation spectrum recorded under jet-cooled conditions with about 0.8 cm^{-1} resolution, which we estimated from the resolution of the fundamental output, 0.45 cm^{-1}, of their laser. In their report the uncertainties associated with the parameters were not reported either, even though the rotational line-widths have relatively large uncertainties ($\pm$0.3—3.0 cm^{-1}). Since the uncertainties of these parameters were not reported in Refs. 5 and 14, it would be difficult to discuss the difference between our determined values and theirs. However, if we assume uniform uncertainties of $\pm$30% for Γ_0 and α_a reported in Refs. 5 and 14, these data are also consistent with ours.

Table 3. Comparison of Γ_0 and α_a Determined in the Present Study with Those in the Previous Studies

	This work[a)]	Ref. 5[b)]	Ref. 8[b,c)]	Ref. 14[a)]
Γ_0	2.5(1)	3.0	2.1(2)	3.2
α_a	0.63(1)	1.05[d)]	0.74(15)[e)]	1.12[d,e)]
Methods	LIPF	(3+1)MPI	2 photon LIF	(3+1)MPI

a) Measured under jet-cooled conditions. b) Measured in a bulb at room temperature. c) The errors in the parameters were estimated in the present study on the basis of the statement in Ref. 8 that the errors of Γ_0 and C_a were estimated to be about 10%. d) The α_a value was transformed from the line-width expression $\Gamma=\Gamma_0(1+C_aK_a'^2)$ as $\alpha_a=\Gamma_0C_a$. e) The α_a value was transformed from the line-width expression $\Gamma=\Gamma_0(1+C_a\langle J_a'^2\rangle)$ as $\alpha_a=\Gamma_0C_a$.

We used the expectation values $\langle J_a'^2\rangle$ throughout the analysis to describe the rotational dependence of the line-widths, the branching ratios and the spectral intensities. When H_2O molecules are rotationally highly excited, $\langle J_a'^2\rangle$ can be approximated by $K_a'^2$. Therefore, when the rotational temperature is relatively high, $K_a'^2$ can be used in place of $\langle J_a'^2\rangle$ to describe the rotational dependence of the linewidth in Eq. 7. However, at low rotational temperatures as in our case, $K_a'^2$ can no longer be used to describe the rotationally dependent predissociation process. Indeed, in Fig. 1(a) the rotational transitions $6_{0,6}$–$6_{1,6}$ and $4_{0,4}$–$4_{1,4}$ having $K_a'=0$ were identified at 80583.5 and 80600.4 cm^{-1}, respectively, showing clearly that the K_a' description is not appropriate.

Previously Hodgson et al.[9] derived the branching ratio β_2 to form the excited $OH(A^2\Sigma^+)$ photofragments from the $\tilde{B}^1A_1$ state as $\beta_2=\exp(-0.1\langle J_a'^2\rangle)$ from the simulation of the rotational contour of the two-photon excitation spectrum at room temperature. Their parameter, 0.1, in the exponent was found to be very close to our determined corresponding parameter, γ=0.097(7), in $\exp(-\gamma\langle J_a'^2\rangle)$.

4. Absolute Cross Section of OH(A) Production. The quantitative data for the OH production cross section after the photodissociation of H_2O are important for the understanding of photochemistry occurring in the interstellar medium as well as in the earth's atmosphere, where reactive OH radicals play a central role. The relative cross section of OH(A) production can be derived from the results of our present spectral analysis. For the i-th rotational transition, its integrated absorption cross section I_A^i is proportional to the rotational transition factor S_i, which can be evaluated using the rotational constants of the $\tilde{X}(0,0,0)$[29] and $\tilde{C}(0,0,0)$[1] levels, i.e.

$$I_A^i = CS_i, \tag{15}$$

where C denotes a constant factor for the $\tilde{C}$–$\tilde{X}$ origin band. On the other hand, the absorption cross section $\sigma_{abs.}^i$ is expressed as,

$$\sigma_{abs.}^i(\omega) = I_A^iL(\omega,\omega_i), \tag{16}$$

where $L(\omega,\omega_i)$ is the absorption line profile defined by Eq. 11. Therefore, the corresponding OH(A) production cross section $\sigma_{OH(A)}^i$ can be represented by multiplying the absorption cross section $\sigma_{abs.}^i$ with the branching ratio of Channel (1b) described by Eq. 13 as,

$$\sigma^{i}_{OH(A)}(\omega) = \sigma^{i}_{abs.}(\omega)\frac{\alpha_a\langle J'^2_a\rangle}{\Gamma_0 + \alpha_a\langle J'^2_a\rangle}e^{-0.097\langle J'^2_a\rangle}$$

$$= CS_i\frac{\alpha_a\langle J'^2_a\rangle}{\Gamma_0 + \alpha_a\langle J'^2_a\rangle}e^{-0.097\langle J'^2_a\rangle}L(\omega, \omega_i), \quad (17)$$

using Γ_0 and α_a obtained in our measurements.

The coefficient C was determined using the relationship $f=2.6\times10^{-3}\ I_A$ (Mb cm^{-1})[30] and Eq. 15 with the absorption oscillator strengths f for transitions $2_{1,1}$–$1_{0,1}$, $1_{1,1}$–$1_{0,1}$, $3_{1,3}$–$3_{0,3}$, $2_{0,2}$–$3_{1,2}$, and $2_{1,1}$–$3_{2,1}$ reported by Smith et al.[31] with experimental uncertainties of ±20%. Then, according to Eq. 17 the absolute OH(A) cross section was determined as a function of the excitation wavenumber and is plotted in Fig. 6. By taking account of the fluctuation of the five C values derived from the five f values and the uncertainties associated with the f values, we estimate the uncertainty of the C value to be ±30%. The derived cross section data also have the same amount of uncertainties.

Lee et al.[32] measured the absolute OH(A) production cross section at 124.28 and 123.88 nm using a spark-discharge light source with a bandwidth of 0.75 nm (ca. 97 cm^{-1}) at room temperature. For comparison, their results are plotted in Fig. 6 with asterisks. Since the bandwidth of their light source is broad (ca. 97 cm^{-1}) and many rotational levels can be excited simultaneously, the reported cross sections should be regarded as values averaged over the rotational transitions covered by the bandwidth of the light. Considering the estimated uncertainties associated with our present $\sigma_{OH(A)}$ values, the two cross sections obtained by Lee et al. are in good agreement with ours.

Summary and Conclusion

Rotationally dependent and rotationally independent photodissociation pathways via the $\tilde{C}^1B_1$ state of H_2O have been investigated by measuring the rotational structure of LIPF spectra of the $\tilde{C}^1B_1$–$\tilde{X}^1A_1$ origin band transition in a wavelength range of 124.3—123.7 nm under jet-cooled conditions. Due to low rotational temperature achieved by the supersonic jet cooling and the high-resolving power of the tunable VUV laser, the LIPF spectra were simplified significantly and exhibited a well-resolved rotational structure, which enabled us to measure the linewidth of the individual rotational transitions. The broadened width Γ of the rotational transition peaks was found to be represented well by the simple formula: $\Gamma=\Gamma_0+\alpha_a\langle J'^2_a\rangle$, with two optimized parameters $\Gamma_0=2.5(1)$ cm^{-1} and $\alpha_a=0.63(1)$ cm^{-1}. The rotationally independent dissociation, whose contribution is represented by Γ_0, was considered to occur through the vibronic coupling with nearby $^1B_1$ electronic state to form OH fragments in its electronic ground $X^2\Pi$ state. On the other hand, the rotationally dependent term was regarded as the contribution from the a-axis orbital-rotation interaction with the $\tilde{B}^1A_1$ state, from which the electronically excited OH($A^2\Sigma^+$) fragments as well as the electronic ground OH($X^2\Pi$) fragments are produced. The branching ratio to form the $\tilde{B}^1A_1$ state, β_1, is represented by $\beta_1=\alpha_a\langle J'^2_a\rangle/(\Gamma_0+\alpha_a\langle J'^2_a\rangle)$. From the least-squares fit to the intensity profiles of the LIPF spectra at five different rotational temperatures, the branching ratio of the OH(A) formation via the $\tilde{B}^1A_1$ state was expressed by an exponential form: $\beta_2=\exp(-\gamma\langle J'^2_a\rangle)$, with $\gamma=0.097(7)$. Then, the branching ratios for the three different dissociation channels were obtained using β_1 and β_2 as a function of $\langle J'^2_a\rangle^{1/2}$. Finally, the absolute cross sections to produce the electronically excited photofragments OH(A) were evaluated using the literature values for the absorption oscillator strength of the five rotational transitions.

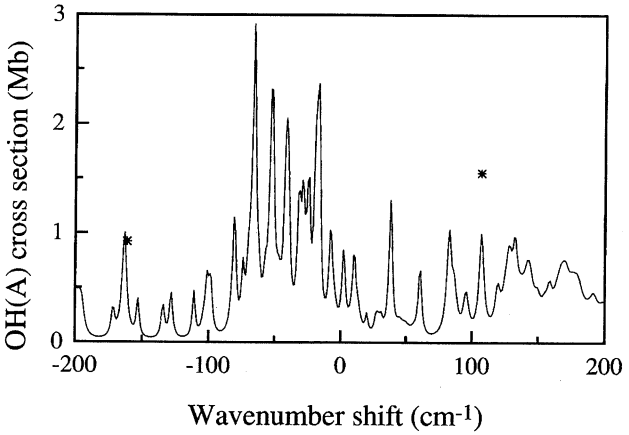

Fig. 6. Absolute cross sections to produce excited OH($A^2\Sigma^+$) fragments as a function of the excitation energy obtained from Eq. 17 using literature values of the absorption oscillator strengths of rotational transitions in Ref. 31. The two cross-sections measured in Ref. 32 using a light source with a broad bandwidth (ca. 97 cm^{-1}) are also plotted with asterisks for comparison. The wavenumber shift is measured from the band origin at 80624.6(4) cm^{-1}.

We thank Mr. T. Kawauchi, Mr. S. Sato, and Mr. N. Hirano (Marubun Co., Ltd.) for their technical support in installing an Infinity (Coherent) OPPO (Lambda Physik) system. We also thank Dr. K. Yoshino, Dr. J. Esmond, and Prof. M. S. Child for their helpful discussions on the photodissociation of H_2O in the vacuum UV region. S. L. acknowledges support from a Japanese Government Scholarship. The present work is supported partly by Grant-in-Aid for Scientific Research (Nos. 05453016 and 08640636) and Grant-in-Aid for Scientific Research on Priority Area (No. 07240106) from Ministry of Education, Science, Sports and Culture, and CREST (Core Research for Evolutionary Science and Technology) fund from Japan Science Technology Corporation.

References

1) J. W. C. Johns, *Can. J. Phys.*, **41**, 209 (1963); *Can. J. Phys.*, **49**, 944 (1971).

2) S. Bell, *J. Mol. Spectrosc.*, **16**, 205 (1964).

3) T. Carrington, *J. Chem. Phys.*, **41**, 2012 (1964).

4) H.-T. Wang, W. S. Felps, and S. P. McGlynn, *J. Chem. Phys.*, **67**, 2614 (1977).

5) M. N. R. Ashfold, J. M. Bayley, and R. N. Dixon, *Chem. Phys.*, **84**, 35 (1984).

6) J. P. Simons, A. J. Smith, and R. N. Dixon, *J. Chem. Soc., Faraday Trans.*, **280**, 1489 (1984).
7) P. Andresen, G. S. Ondrey, B. Titze, and E. W. Rothe, *J. Chem. Phys.*, **80**, 2548 (1984).
8) G. Meijer, J. J. terMeulen, P. Andresen, and A. Bath, *J. Chem. Phys.*, **85**, 6914 (1986).
9) A. Hodgson, J. P. Simons, M. N. R. Ashfold, J. M. Bayley, and R. N. Dixon, *Mol. Phys.*, **54**, 351 (1985).
10) M. P. Docker, A. Hodgson, and J. P. Simons, *Mol. Phys.*, **57**, 129 (1986).
11) H. J. Krautwald, L. Schnieder, K. H. Welge, and M. N. R. Ashfold, *Faraday Discuss. Chem. Soc.*, **82**, 99 (1986).
12) M. Broudard, M. P. Docker, A. Hodgson, and J. P. Simons, *J. Chem. Phys.*, **86**, 7246 (1987).
13) V. Engel, G. Meijer, A. Bath, P. Andresen, and R. Schinke, *J. Chem. Phys.*, **87**, 4310 (1987).
14) H.-H. Kuge and K. Kleinermanns, *J. Chem. Phys.*, **90**, 46 (1989).
15) M. V. Dirke, B. Heumann, R. Schinke, R. J. Sension, and B. S. Hudson, *J. Chem. Phys.*, **99**, 1050 (1993).
16) D. H. Mordaunt, M. N. R. Ashfold, and R. N. Dixon, *J. Chem. Phys.*, **100**, 7360 (1994).
17) F. Flouquet and J. A. Horsley, *J. Chem. Phys.*, **60**, 3767 (1974).
18) E. Segev and M. Shapiro, *J. Chem. Phys.*, **77**, 5604 (1982).
19) G. Theodorakopoulos, I. D. Petsalakis, and R. J. Buenker, *Chem. Phys.*, **96**, 217 (1985).
20) R. N. Dixon, *Mol. Phys.*, **54**, 333 (1985).
21) V. Engel, R. Schinke, and V. Staemmler, *Chem. Phys. Lett.*, **130**, 413 (1986).
22) D. M. Hirst, and M. S. Child, *Mol. Phys.*, **77**, 463 (1992).
23) R. N. Dixon, *J. Chem. Phys.*, **102**, 301 (1995).
24) F. Schneider, F. Di Giacomo, and F. A. Gianturco, *J. Chem. Phys.*, **104**, 5153 (1996).
25) S. G. Tilford and J. D. Simmons, *J. Phys. Chem. Ref. Data*, **1**, 147 (1972).
26) K. Yamanouchi and S. Tsuchiya, *J. Phys. B*, **28**, 133 (1995).
27) C. D. Pibel, K. Yamanouchi, and S. Tsuchiya, *J. Chem. Phys.*, **100**, 195 (1994).
28) K. Yamanouchi, K. Ohde, A. Hishikawa, and C. Pibel, *Bull. Chem. Soc. Jpn.*, **68**, 2459 (1995); A. Hishikawa, K. Onde, R. Itakura, S. Liu, K. Yamanouchi, and K. Yamashita, *J. Phys. Chem.*, **101**, 694 (1997).
29) J.-M. Flaud and C. Camy-Petret, *Mol. Phys.*, **32**, 499 (1976).
30) A. Rauk and J. M. Barriel, *Chem. Phys.*, **25**, 409 (1977).
31) P. L. Smith, K. Yoshino, H. E. Griesinger, and J. H. Black, *Astrophys. J.*, **250**, 166 (1981).
32) L. C. Lee, L. Oren, E. Phillips, and D. L. Judge, *J. Phys. B*, **11**, 47 (1978).